

# Development of a Novel SPECT Tracer to Image c-Met Expression in Non-Small Cell Lung Cancer in a Human Tumor Xenograft

Zhaoguo Han<sup>1,2†</sup>, Yadi Xiao<sup>1,2†</sup>, Kai Wang<sup>1,2</sup>, Ji Yan<sup>1,2</sup>, Zunyu Xiao<sup>1,2</sup>, Fang Fang<sup>1,2</sup>, Zhongnan Jin<sup>1,2</sup>, Yang Liu<sup>1,2</sup>, Xilin Sun<sup>\*1,2,3</sup>, Baozhong Shen<sup>\*1,2</sup>

## Affiliations:

<sup>1</sup>Molecular Imaging Research Center, Harbin Medical University, Harbin, Heilongjiang, China.

<sup>2</sup>TOF-PET/CT/MR center, The Fourth hospital of Harbin Medical University, Harbin, Heilongjiang, China.

<sup>3</sup>Molecular Imaging Program at Stanford (MIPS), Department of Radiology, Stanford University School of Medicine, Stanford, California, USA.

†: Equal contributors

## Corresponding Author

*Primary:* Baozhong Shen, MD, PhD, Molecular Imaging Research Center, Harbin Medical University, 766Xiangan N street, Songbei District, Harbin, Heilongjiang, China, 150028, E-mail: shenbz@ems.hrbmu.edu.cn, Fax: +86-451-82576509. *Secondary:* Xilin Sun, PhD, Molecular Imaging Research Center, Harbin Medical University, 766Xiangan N street, Songbei District, Harbin, Heilongjiang, China, 150028, E-mail: sunxilin@aliyun.com, Fax: +86-451-82576509.

**First Author:** Zhaoguo Han, Doctoral students, Molecular Imaging Research Center, Harbin Medical University, 766Xiangan N street, Harbin, Heilongjiang, China, 150028, e-mail: 18846782876@163.com, fax: +0-860-451-82576509.

**Word count:** 4840

**Financial support:** This work was supported partly by the National Natural Science Foundation of China (81471724, 81627901, 31210103913, 81101088, 81130028), National Basic Research Program of China (2015CB931800), Heilongjiang Province Foundation for Returned Overseas Chinese Scholars, and the Key Laboratory of Molecular Imaging Foundation(College of Heilongjiang Province).

**Running title:** c-Met targeted imaging

## ABSTRACT

**Rationale:** Elevated expression of the c-Met receptor plays a crucial role in cancers. In non-small cell lung cancer (NSCLC), aberrant activation of c-Met signaling pathway contributes to tumorigenesis and cancer progression, and may mediate acquired resistance to epidermal growth factor receptor-targeted therapy. c-Met is therefore emerging as a promising therapeutic target for treating NSCLC, and the methods for noninvasive *in vivo* assessment of c-Met expression will improve NSCLC treatment and diagnosis.

**Methods:** A new peptide-based (cMBP) radiotracer targeting c-Met, <sup>99m</sup>Tc-hydrazine nicotinamide (HYNIC)-cMBP, was developed for single photon emission computed tomography (SPECT) imaging. Cell uptake assays were performed on two NSCLC cell lines with different c-Met expression: H1993 (high expression) and H1299 (no expression). *In vivo* tumor specificity was assessed by SPECT imaging in tumor-bearing mice at 0.5, 1, 2 and 4 h after injection of the probe. Blocking assays, biodistribution and autoradiography were also conducted to determine probe specificity.

**Results:** <sup>99m</sup>Tc-HYNIC-cMBP was prepared with high efficiency and showed higher uptake in H1993 cells than H1299 cells. Biodistribution and autoradiography also showed significantly higher accumulation of <sup>99m</sup>Tc-HYNIC-cMBP in H1993 tumors than H1299 (H1993: 4.74±1.43 %ID/g and H1299: 1.00±0.37 %ID/g at 0.5h, *p*<0.05). H1993 tumors were clearly visualized at 0.5h in SPECT images, whereas H1299 tumors were not observed at any time. Specificity of <sup>99m</sup>Tc-HYNIC-cMBP to c-Met was demonstrated by competitive block with excess un-radiolabeled peptide.

**Conclusion:** We developed a novel SPECT tracer,  $^{99m}\text{Tc}$ -HYNIC-cMBP, for c-Met-targeted imaging in NSCLC that specifically bound to c-Met with favorable pharmacokinetics *in vitro* and *in vivo*.

**Key words:** c-Met; targeted peptide; NSCLC; SPECT

# INTRODUCTION

c-Met is a receptor tyrosine kinase encoded by a proto-oncogene (1). Upon binding of hepatocyte growth factor, active c-Met stimulates various signaling pathways implicated in cellular processes, including cell proliferation, motility and apoptosis (2). Aberrantly high expression of c-Met resulting from gene amplification and protein overexpression increases c-Met activation and oncogenic transformation (3). Elevated c-Met expression has been observed in many cancers, including thyroid, pancreatic, and lung cancer (4).

Lung cancer has the highest incidence and mortality rates worldwide (5), and non-small cell lung cancer (NSCLC) accounts for about 80% of lung cancers (6). High expression of c-Met has been detected in many NSCLCs, and is thought to play an important role in promoting tumorigenesis and cancer progression (7). Activation of hepatocyte growth factor /c-Met downstream signaling by the phosphatidylinositol 3 kinase/protein kinase B and mitogen-activated protein kinase pathways can promote tumor growth, metastasis, angiogenesis, and apoptosis inhibition, which contribute to invasiveness and poor prognosis in NSCLC. Furthermore, c-Met gene amplification is a significant mechanism mediating resistance to therapies targeting epidermal growth factor receptor in NSCLC (8, 9).

Studies suggest that c-Met is an effective drug target for treating NSCLC (10) and combination therapies targeting c-Met and epidermal growth factor receptor have attracted attention in the clinical setting (11). However, limitations in early detection challenge the overall efficacy of cancer treatment. Typically, methods screening for lung cancer, e.g. computerized tomography, detect tumors mostly at middle or advanced stages (12). Diagnoses for lung cancer

currently rely on biopsies with multiple disadvantages including a risk of pleural metastasis, patient intolerance, and sampling inaccuracy due to tumor heterogeneity (13). It is therefore desirable to develop more precise and less invasive methods to diagnose lung cancer, particularly at early stages.

Molecular imaging is a noninvasive method for qualitative and quantitative information on tumor-associated molecular targets *in vivo*. Over decades, c-Met has increasingly been utilized as a biomarker for molecular imaging. Despite significant advances in c-Met-targeted imaging, problems remain. For instance, an anti-c-Met monoclonal antibody DN30 (~150 kDa) labeled with  $^{89}\text{Zr}$  provided quantitative images with high uptake in gastric cancer. However, the tracer had prolonged circulation and slow clearance, which reduced tumor-to-background contrast and lead to very late optimal imaging times (3-5 days) (14). Another anti-cMet diabody (~55 kDa) labeled with  $^{89}\text{Zr}$  achieved acceptable images, but also showed slow clearance (15). These examples highlight the disadvantages of antibody-based tracers: long biological half-life and slow clearance.

More recent imaging strategies using peptide targeting have received greater attention by overcoming most limitations of antibody-based tracers. Indeed, peptide-based tracers have smaller size, simpler synthesis, faster clearance, and lower risk of immunogenicity (16). GE-137 (~4.2 kDa), a c-Met-targeted peptide labeled with cyanine dye, produced encouraging results in detecting malignant polyps in high-risk colon cancer patients by optical imaging (17). Based on same targeted peptide to GE-137,  $^{18}\text{F}$ -AH113804 also successfully assessed locoregional recurrence of breast cancer (18).

$^{99m}\text{Tc}$  is widely used in nuclear medicine. To our knowledge,  $^{99m}\text{Tc}$ -labeled peptides targeting c-Met have not been studied in NSCLC. cMBP (KSLSRHDHIIHHH) is a c-Met binding peptide identified through phage display screening that was previously labeled with a fluorescent dye to detect c-Met in U87MG glioblastoma (19, 20). Here, cMBP was modified with a bifunctional chelator, hydrazine nicotinamide (HYNIC), for labeling with  $^{99m}\text{Tc}$  ( $t_{1/2}=6.02$  h) ( $^{99m}\text{Tc}$ -HYNIC-cMBP) and used to assess c-Met expression in NSCLC by single photon emission computed tomography (SPECT).

## MATERIALS AND METHODS

### Radiosynthesis of $^{99m}\text{Tc}$ -HYNIC-cMBP

ChinaPeptides Co., Ltd (Shanghai, China) synthesized HYNIC-cMBP and cMBP, which was radiolabelled with  $^{99m}\text{Tc}$  ( $^{99m}\text{Tc}$ -HYNIC-cMBP) as previously described (21). Briefly, 5  $\mu\text{g}$  HYNIC-cMBP was added to ethylenediamine-N,N'-diacetic acid (10mg)/tricine (20 mg) in 1ml phosphate buffer solution (PBS, pH 6-7), followed by 0.5 ml  $^{99m}\text{TcO}_4$  solution (370 MBq) and 20  $\mu\text{L}$  of tin-II solution (10 mg  $\text{SnCl}_2$  in 10mL 0.1 N HCL). All reagents were purchased from Sigma. The mixture was heated (85°C, 15min, nitrogen protection) then cooled to room temperature. Reaction mixture was purified with Sep-Pak C18 plus cartridge (Waters) and the radiolabelled peptide was collected.

The partition coefficient of  $^{99m}\text{Tc}$ -HYNIC-cMBP was measured in octanol and saline system. 7.4 MBq of  $^{99m}\text{Tc}$ -HYNIC-cMBP was mixed with the octanol (0.5 ml) and saline (0.5 ml) system for 1 h. Then the mixture was centrifugated (3,000 rpm, 5 min) and activity from each layer (take

samples of 100  $\mu$ l) was counted using a gamma counter (PerkinElmer 2480).

### **Cell Culture**

Two NSCLC cell lines were selected: H1993 (high c-Met expression) and H1299 (no c-Met expression) and cultured as previously reported (22).

### **Determination of Dissociation Constant (Kd)**

High c-Met expressing H1993 cells were used in a saturation binding experiment to determine the Kd of  $^{99m}\text{Tc}$ -HYNIC-cMBP (23). Briefly, H1993 cells were seeded in two 24-well plates at  $0.2 \times 10^6$  cells/well 24 h prior. A stock solution of  $^{99m}\text{Tc}$ -HYNIC-cMBP was diluted with media to six concentrations (1, 10, 40, 80, 100 and 160 nM). Increasing concentrations of tracer were added to the wells of one plate to assess cell-bound activity, and nonspecific binding was determined in another plate by adding non-radiolabeled cMBP (100  $\mu$ M). After incubation for 0.5 h at 4 °C, the tracer was removed. Cells were washed with cold PBS and activity was measured. Specific binding was calculated by subtracting nonspecific binding from cell-bound activity. Kd was determined from specific binding curve using nonlinear regression curve fits (Graphpad Prism 5 software).

### **Cellular Uptake and Internalization**

$^{99m}\text{Tc}$ -HYNIC-cMBP cellular uptake and blocking with non-radiolabeled cMBP were performed at 15, 30, 60, 120 and 240 min as previously reported (22).

c-Met positive H1993 cells were used to evaluate whether  $^{99m}\text{Tc}$ -HYNIC-cMBP was internalized (24). Briefly, H1993 cells were seeded in 12-well plates ( $5 \times 10^5$  cells). After 24 h,  $^{99m}\text{Tc}$ -HYNIC-cMBP was added (37 KBq/ml) and incubated for different times. Free

$^{99m}\text{Tc}$ -HYNIC-cMBP was removed and washed cells with ice-cold PBS followed by 0.2 M glycine buffer in 4 M urea (pH 2.5) for 5 min on ice to determine membrane-bound activity. Next, cells were harvested using 1 N NaOH to determine internalized activity. Results were presented as internalization percent of cell-associated activity (membrane-bound + internalization).

### **Animal Xenograft Models**

Female BALB/c nude mice (5-6 weeks, 19-23 g) were implanted subcutaneously with H1993 or H1299 ( $5 \times 10^6$  cells) in the right shoulder. Tumor volume was measured by caliper until reaching  $\sim 500 \text{ mm}^3$  (approximately 5-6 weeks). All animal experiments were approved by the Harbin Medical University Animal Ethics Committee in accordance with Chinese legislation and followed relevant guidelines. The institutional review board approved this study in mice with NSCLC tumor xenografts.

### **In Vitro and In Vivo Stability**

Radiochemical purity of  $^{99m}\text{Tc}$ -HYNIC-cMBP incubated in either mouse serum or PBS at  $37^\circ\text{C}$  was measured for 0, 0.5, 1, 2 and 4 h.  $^{99m}\text{Tc}$ -HYNIC-cMBP was collected and diluted with PBS, at baseline 0.37 MBq in 0.5ml solution A ( $V_{\text{water}} : V_{\text{Trifluoroacetic Acid}} = 99.9 : 0.1$ ) and radiochemical purity was measured by radio-high performance liquid chromatography (HPLC). At subsequent timepoints, the probe samples were added to 0.5 ml of dimethyl formamide to precipitate protein. After centrifugation, the supernatant was diluted with 0.5 ml of solution A and analyzed with HPLC.

*In vivo* stability was determined with procedure as described previously (25). Briefly, H1993 tumor-bearing mice were injected with  $^{99m}\text{Tc}$ -HYNIC-cMBP (11.1 MBq in 150  $\mu\text{L}$  saline) and

ethanized at 1 h after. Blood and urine were collected and immediately centrifuged to remove blood cells. Plasma and urine were added into 0.5 ml of 1% Triton X-100 in dimethyl formamide for further centrifugation. Then supernatant portions of each samples were diluted with 0.5 ml solution A for radio-HPLC analysis. Tumors and liver were homogenized with 0.5 ml of 1% Triton X-100 (Sigma) in dimethyl formamide then centrifuged. The supernatants were diluted with 0.5 ml solution A for radio-HPLC analysis. Radio-HPLC (GX-281, Gilson, France) utilized C18 column (10  $\mu$ m, 19  $\times$  250 mm, Waters) with mobile phase of 50% ethanol at flow rate of 5 ml/min. Eluted fractions were collected 30 s/tube for measuring radioactivity and the resultant radio-HPLC chromatogram was plotted.

### **In Vivo SPECT Imaging**

SPECT scanning of tumor-bearing mice (injected with 8.51 MBq  $^{99m}\text{Tc}$ -HYNIC-cMBP) was performed with a clinical SPECT scanner (Discovery 670H3100NA, GE healthcare), equipped with low-energy, low energy high-resolution collimators with parallel pinholes. All images were obtained through detector 1 for anterior static scanning (100 counts), zoom factor of 1.00, and stored with resolution 1024  $\times$  1024. The energy window setting was 140 keV. Image analysis was performed with an Xeleris Functional imaging Workstation (version 3.1). The ratio of counts in the tumor to contralateral tissue (T/C) was calculated over the regions-of-interest.

### **Biodistribution and Pharmacokinetics**

The tumor bearing mice were injected with 1.85 MBq  $^{99m}\text{Tc}$ -HYNIC-cMBP and euthanized at serial points for biodistribution (22).

Pharmacokinetics of  $^{99m}\text{Tc}$ -HYNIC-cMBP was evaluated as described (26) with

modifications. Mice were euthanized and blood (100  $\mu$ l) was drawn by cardiac puncture at 3, 9, 15, 30, 45, 60 and 120 min after injection. Blood was centrifugated to collect the plasma. The plasma (extracted at 30 min) was mixed with 10% sulphosalicylic acid to precipitate protein. Activity of protein precipitate and supernatant were measured, and time-logarithmic versus plasma activity curve was plotted. Tracer eliminated followed first-order reaction kinetics and the elimination rate constant ( $K_{el}$ ) was calculated as the negative slope of linear part of plotted curve. The elimination half-life was calculated as  $\ln(2)/$ elimination rate constant ( $K_{el}$ ).

### **Blocking Assays**

For blocking assays in SPECT imaging and biodistribution, non-radiolabelled cMBP was pre-injected into H1993 xenografts at 100 mg/Kg body weight 1 h before injection of the  $^{99m}\text{Tc}$ -HYNIC-cMBP.

### **Autoradiography**

Tumor-bearing mice were euthanized at 0.5 h after injection. Tumors were excised and embedded within OCT (optimal cutting temperature compound) freezing at  $-80^{\circ}\text{C}$ . Autoradiography, hematoxylin and eosin and immunofluorescence staining were performed on consecutive tumor sections (10  $\mu\text{m}$ ). Sections were exposed to photoreceptive film for 24h, then imaged with Cyclone® Plus storage phosphor system (PerkinElmer, USA).

### **Western Blot and Immunofluorescence**

Western blot and immunofluorescence experiments were performed as previously reported (22). Concentration of anti-c-Met primary antibody (Abcam-ab51067) was 1:1000 for western blot and 1:100 for immunofluorescence.

## **Statistical Analysis**

All data are expressed as mean  $\pm$  standard deviation (n=3). Statistical analyses were carried out using GraphPad Prism 5 software. Statistical differences between the groups were estimated by using the *t* test. *P*-value < 0.05 was considered statistically significant.

## **RESULTS**

### **Radiosynthesis and Characterization of <sup>99m</sup>Tc-HYNIC-cMBP**

The process of radiochemical synthesis and specific binding to c-Met of <sup>99m</sup>Tc-HYNIC-cMBP is illustrated in Supplemental Figs. 1A and 1B. The product was obtained with yield of  $\geq 75\%$  and a radiochemical purity of  $>98\%$  after purification. The logP value obtained was  $-3.003 \pm 0.48$  indicating the probe was water-soluble.

### **Determination of Kd**

Cell binding affinity of <sup>99m</sup>Tc-HYNIC-cMBP to H1993 cells was determined by its specific binding curve (Fig. 1A) to have a Kd of  $56.30 \pm 2.11$ . According to reported theory, Kd value of <sup>99m</sup>Tc-HYNIC-cMBP exhibited moderate affinity (1 nM~1  $\mu$ M) (27) suggesting that <sup>99m</sup>Tc-HYNIC-cMBP would be effective as a tumor c-Met radiotracer.

### **Cellular Uptake and Blocking Assays**

Cellular uptake and blocking assays of H1993 and H1299 cells were shown (Fig. 1B). There was a rapid uptake of <sup>99m</sup>Tc-HYNIC-cMBP which peaked at 30 min in H1993 cells. The tracer subsequently decreased gradually at 60, 120 and 240 min. In contradistinction, visibly lower cellular uptake was noted in the H1299 cells with no obvious uptake trend was observed. The

accumulation of  $^{99m}\text{Tc}$ -HYNIC-cMBP in H1993 cells reached its highest level ( $0.68\pm 0.06\%$  of total input activity) at 30 min, about 2.4-fold higher than H1299 cells ( $p<0.01$ ). In blocking assays with excess un-radiolabelled cMBP, uptake of  $^{99m}\text{Tc}$ -HYNIC-cMBP in H1993 cells at 30 min was lower ( $0.33\pm 0.06\%$ ,  $p<0.01$ ). Uptake in H1299 cells remained unchanged. These results suggested that  $^{99m}\text{Tc}$ -HYNIC-cMBP bound specifically to c-Met expressed H1993 cells.

Internalization results (Supplemental Fig. 2) indicated that  $^{99m}\text{Tc}$ -HYNIC-cMBP was internalized in c-Met positive H1993 cells. The tracer exhibited an increasing trend of internalization rate with a maximum of  $10.21\pm 0.46\%$  cell-associated activity at 120 min followed by a plateau.

#### **In Vitro and In Vivo Stability Assays**

According to radio-HPLC analyses, retention time of  $^{99m}\text{Tc}$ -HYNIC-cMBP was 6.5 min and more than 98% of the tracer remained intact during 0-4 h incubation in mouse serum and PBS (Supplemental Figs. 3A and 3B). Results showed that  $^{99m}\text{Tc}$ -HYNIC-cMBP was highly stable *in vitro*. *In vivo* stability measured by radio-HPLC under identical conditions is shown in Figs. 2A, 2B, 2C and 2D. At 1 h intact tracer in plasma and tumor was 98% and 96%, respectively. Intact tracer measured in liver and urine was 40% and 54%, respectively. These results suggested excellent *in vivo* stability of  $^{99m}\text{Tc}$ -HYNIC-cMBP with expected degradation through hepatobiliary and urinary systems.

#### **In Vivo SPECT Imaging and Blocking Assays**

$^{99m}\text{Tc}$ -HYNIC-cMBP provided effective SPECT imaging of c-Met-positive H1993 tumors (Fig. 3A, top row) with H1299 tumors serving as a negative control (Fig. 3A, bottom row).

Quantitative analyses of the region of interest expressed as tumor-to-contralateral (T/C) ratios are shown in Fig. 3B.

H1993 xenografts were clearly visualized by SPECT imaging at 0.5 h, with highest T/C ratio of  $2.60 \pm 0.35$ , while H1299 xenografts were not detected (T/C ratio  $1.22 \pm 0.22$ ). H1993 xenografts remained detectable at 1 h, but the T/C ratio decreased to  $1.90 \pm 0.13$ .  $^{99m}\text{Tc}$ -HYNIC-cMBP cleared from tumors within 2 to 4 h, likely because the tracer lacked lipophilicity. Thus, 0.5 h was optimum imaging time for  $^{99m}\text{Tc}$ -HYNIC-cMBP in NSCLC. In H1299 xenografts, no obvious tumor activity was detected over time with T/C ratios ranging from  $1.13 \pm 0.09$ ~ $1.29 \pm 0.10$ , consistent with negligible c-Met expression. Highest activity was observed in the kidney and bladder, indicating that  $^{99m}\text{Tc}$ -HYNIC-cMBP was primarily cleared via the urinary system.

Representative SPECT images and quantitative analyses for blocking experiments are shown in Figs. 4A and 4B. After pretreatment with excess of non-radiolabelled cMBP, H1993 xenografts were difficult to discern in images. Consistently,  $^{99m}\text{Tc}$ -HYNIC-cMBP accumulation in pretreated-H1993 tumors was significantly lower (T/C ratios of  $1.29 \pm 0.11$ ). Collectively, these results support that  $^{99m}\text{Tc}$ -HYNIC-cMBP specifically accumulated in c-Met-positive H1993 xenografts *in vivo*.

### **Biodistribution and Pharmacokinetics**

To confirm the SPECT imaging results, the biodistribution of  $^{99m}\text{Tc}$ -HYNIC-cMBP was assessed in mice bearing H1993 and H1299 xenografts. As shown in Supplemental Tables 1 and 2 and Fig. 5, H1993 xenograft highest uptake was at 0.5 h ( $4.74 \pm 1.43$  %ID/g) then decreased at 1 h ( $2.84 \pm 0.28$  %ID/g), and further declined at 2 and 4 h ( $0.87 \pm 0.13$  %ID/g and  $0.75 \pm 0.14$  %ID/g,

respectively). In contradistinction, tumor uptake in H1299 xenografts was significantly lower at 0.5 and 1 h ( $1.00\pm 0.37$  %ID/g and  $0.71\pm 0.13$  %ID/g, respectively). Uptake in non-target-tissues was similar in H1993 and H1299 xenograft-bearing mice. Highest signal was obtained in kidney at 0.5 h ( $252.66\pm 44.37$  %ID/g in H1299 and  $247.55\pm 40.52$  %ID/g in H1993), then decreased over time, further suggesting that  $^{99m}\text{Tc}$ -HYNIC-cMBP was rapidly cleared through the urinary system. Blocking assays demonstrated that uptake was significantly reduced in H1993 xenografts ( $1.02\pm 0.43$  %ID/g) with excess non-radiolabelled cMBP. Probe uptake for different organs did not differ ( $p>0.05$ ) between H1993 and H1993-block group, excluding the tumors ( $p<0.05$ ).

Protein/plasma and supernatant/plasma activity, protein/plasma binding ratio of  $^{99m}\text{Tc}$ -HYNIC-cMBP to total plasma activity was determined as  $0.10\pm 0.02$  at 30 min. The time-logarithmic value of plasma activity curve was plotted (Supplemental Fig. 4), and elimination rate constant ( $K_{el}$ ) calculated as  $0.02\pm 0.00$  1/min. The elimination half-life was  $32.80\pm 4.21$  min.

### **Autoradiography**

The radioactive exposure, hematoxylin and eosin and immunofluorescence stainings of consecutive tumor sections are presented in Fig. 6. The results revealed preferential accumulation of  $^{99m}\text{Tc}$ -HYNIC-cMBP in H1993 tumors, whereas no accumulation was found except for background signal in H1299 tumors, which only showed background activity, demonstrating that  $^{99m}\text{Tc}$ -HYNIC-cMBP specifically binds to c-Met-positive tumors. Importantly, intra-tumoral distribution of  $^{99m}\text{Tc}$ -HYNIC-cMBP in H1993 tumor sections reflected tumor heterogeneity of NSCLC.

## **In Vitro Assays**

Confirmed by western blots, high c-Met expression was detected in H1993 cells and xenografts, but not in H1299 cells and xenografts (Supplemental Figs. 5A and 5B ). Similarly, significantly higher intensity of fluorescence signal was observed by immunostaining in H1993 cells, whereas negligible signal was in H1299 cells (Supplemental Fig. 5C).

## **DISCUSSION**

Over the decades, c-Met has emerged as a promising therapeutic tumor target in tumor (28). Various molecular imaging strategies evaluating c-Met expression in cancers have been reported (29), which can be classified mainly as antibody-based or peptide-based imaging agents. Although antibody-based c-Met-targeted imaging has been widely researched, inherent limitations including large size, weak tissue penetration, prolonged clearance and potential immunogenicity diminished its utility (30).

Low molecular weight peptides offer many advantages in molecular imaging, including more favorable pharmacokinetics and tissue penetration, lower risk of immunogenicity and toxicity, and flexible in chemical modification (16, 31). To date, the only c-Met-targeted probe in clinical trial is GE-137, a fluorescently labeled c-Met-specific peptide that has been used successfully to detect malignant polyps in patients at high risk of colon cancer (17). While optical imaging is mainly applied to detect superficial tissue externally or in endoscopic procedures and nuclear imaging is more useful in whole body imaging.

In this study, the feasibility of <sup>99m</sup>Tc-HYNIC-cMBP for detecting NSCLC by SPECT

imaging was investigated. As mediating resistance to epidermal growth factor receptor-targeted therapy in NSCLC (7, 8), c-Met-imaging could provide a new strategy to NSCLC diagnosis and treatment.

With a molecular weight of only ~1.6 kDa, cMBP was significantly smaller than monoclonal antibodies (~150 kDa) or derivatives (19, 20). Moreover, as compared to other positron radionuclide-labeled tracers radiolabeling with  $^{99m}\text{Tc}$  was simple with high yield and lower cost. Our results indicated  $^{99m}\text{Tc}$ -HYNIC-cMBP is a promising radiotracer for targeting c-Met *in vivo* and *in vitro*. When compared to other previously reported tracers targeting c-Met (*e.g.*

18.1±4.5%ID/g for  $^{89}\text{Zr}$ -DN30 in GTL-16 gastric cancer and 3.4±0.3%ID/g for

$^{89}\text{Zr}$ -DFO-H2cys-diabody in Hcc827-GR NSCLC, when optimal image contrast) (14, 15), the

smaller  $^{99m}\text{Tc}$ -HYNIC-cMBP showed a moderate uptake (4.74±1.43%ID/g). However, H1993

tumors (H1993) were clearly visualized in SPECT images as early as 0.5 h. Additionally,

$^{99m}\text{Tc}$ -HYNIC-cMBP was rapidly cleared via renal system, which is consistent with water-soluble

low molecular weight probes, albeit unattractive for imaging tumors of the urinary system (32,

33). Nevertheless, rapid clearance is a desirable property for diagnostic tracer, as it reduces tissue

exposure to radiation, background noise, and long delays between contrast treatment and image

readout for receptor-targeted imaging. While it is difficult to directly compare c-Met-targeted

tracers due to intrinsic differences in tumor models, peptide-based tracers tend to produce

high-contrast images at earlier time points than antibody-based tracers due to better tissue

penetration and more rapid elimination.

Despite these advantages,  $^{99m}\text{Tc}$ -HYNIC-cMBP had limitations, such as short retention time

in tumors and low resolution of anatomical structures in images. Furthermore, the optimal imaging time of  $^{99m}\text{Tc}$ -HYNIC-cMBP at 30 min may not allow sufficient time for preparation, and it may be preferable to extend this to approximately 1 h, as is the case for  $^{18}\text{F}$ -fluorodeoxyglucose (34). Thus, in future studies  $^{99m}\text{Tc}$ -HYNIC-cMBP efficacy may be improved by introducing an amino octanoic acid to increase peptide lipophilicity (35), or by creating dimers, such as dimeric-RGD peptide (arginine-glycine-aspartic acid) to increase binding affinity (36, 37). Small animal-SPECT imaging may appropriately provide not only anatomic information with higher resolution, but also dynamic imaging with more improved quantitative analysis and pharmacokinetics modeling.

## CONCLUSION

In this study, proof-of-concept for a novel peptide-based tracer targeting c-Met for SPECT imaging is provided.  $^{99m}\text{Tc}$ -HYNIC-cMBP specifically bound to c-Met *in vitro* and *in vivo*. While further modification and optimization is warranted, cMBP-based radiotracers may be translated into the clinic for the selection and monitoring NSCLC patients to receive c-Met-responsive therapy.

**Disclaimer:** The authors declare that no conflict of interest of any nature.

## ACKNOWLEDGMENTS

We thanks Po Yang, Yingxun Zhang, Yali Cui, Yongyi Wu, Feng Chen, Tengchuang Ma for technical support.

## REFERENCES

1. Cooper CS, Park M, Blair DG, et al. Molecular cloning of a new transforming gene from a chemically transformed human cell line. *Nature*. 1984;311:29-33.
2. Trusolino L, Bertotti A, Comoglio PM. MET signalling: principles and functions in development, organ regeneration and cancer. *Nat Rev Mol Cell Biol*. 2010;11:834-848.
3. Gherardi E, Birchmeier W, Birchmeier C, Vande Woude G. Targeting MET in cancer: rationale and progress. *Nat Rev Cancer*. 2012;12:89-103.
4. Birchmeier C, Birchmeier W, Gherardi E, Vande Woude GF. Met, metastasis, motility and more. *Nat Rev Mol Cell Biol*. 2003;4:915-925.
5. Herbst RS, Heymach JV, Lippman SM. Lung cancer. *N Engl J Med*. 2008;359:1367-1380.
6. Wender R, Fontham ET, Barrera E, Jr., et al. American Cancer Society lung cancer screening guidelines. *CA Cancer J Clin*. 2013;63:107-117.
7. Robinson KW, Sandler AB. The role of MET receptor tyrosine kinase in non-small cell lung cancer and clinical development of targeted anti-MET agents. *Oncologist*. 2013;18:115-122.
8. Engelman JA, Zejnullahu K, Mitsudomi T, et al. MET amplification leads to gefitinib resistance in lung cancer by activating ERBB3 signaling. *Science*. 2007;316:1039-1043.
9. Zucali PA, Ruiz MG, Giovannetti E, et al. Role of cMET expression in non-small-cell lung cancer patients treated with EGFR tyrosine kinase inhibitors. *Ann Oncol*. 2008;19:1605-1612.
10. Liu X, Newton RC, Scherle PA. Developing c-MET pathway inhibitors for cancer therapy: progress and challenges. *Trends Mol Med*. 2010;16:37-45.

11. Spigel DR, Edelman MJ, O'Byrne K, et al. Results from the phase III randomized trial of onartuzumab plus erlotinib versus erlotinib in previously treated stage IIIB or IV non-small-cell lung cancer: METlung. *J Clin Oncol.* 2017;35:412-420.
12. de Koning HJ, Meza R, Plevritis SK, et al. Benefits and harms of computed tomography lung cancer screening strategies: a comparative modeling study for the U.S. Preventive Services Task Force. *Ann Intern Med.* 2014;160:311-320.
13. Mendiratta-Lala M, Sheiman R, Brook OR, Gourtsyianni S, Mahadevan A, Siewert B. CT-guided core biopsy and percutaneous fiducial seed placement in the lung: can these procedures be combined without an increase in complication rate or decrease in technical success? *Eur J Radiol.* 2014;83:720-725.
14. Perk LR, Stigter-van Walsum M, Visser GW, et al. Quantitative PET imaging of Met-expressing human cancer xenografts with 89Zr-labelled monoclonal antibody DN30. *Eur J Nucl Med Mol Imaging.* 2008;35:1857-1867.
15. Li K, Tavare R, Zettlitz KA, et al. Anti-MET immunoPET for non-small cell lung cancer using novel fully human antibody fragments. *Mol Cancer Ther.* 2014;13:2607-2617.
16. Lee S, Xie J, Chen X. Peptide-based probes for targeted molecular imaging. *Biochemistry.* 2010;49:1364-1376.
17. Burggraaf J, Kamerling IM, Gordon PB, et al. Detection of colorectal polyps in humans using an intravenously administered fluorescent peptide targeted against c-Met. *Nat Med.* 2015;21:955-961.
18. Arulappu A, Battle M, Eisenblaetter M, et al. c-Met PET imaging detects early-stage locoregional recurrence of basal-like breast cancer. *J Nucl Med.* 2016;57:765-770.
19. Kim K, Hur Y, Ryu EK, et al. A neutralizable epitope is induced on HGF upon its interaction with its receptor cMet. *Biochem Biophys Res Commun.* 2007;354:115-121.
20. Kim EM, Park EH, Cheong SJ, et al. In vivo imaging of mesenchymal-epithelial transition factor (c-Met) expression using an optical imaging system. *Bioconjug Chem.* 2009;20:1299-1306.
21. Yan Y, Xiao ZY, Song Y, et al. (9)(9)mTc-HYNIC-MPG: a novel SPECT probe for targeting mutated EGFR. *Bioorg Med Chem Lett.* 2015;25:1647-1652.
22. Song Y, Xiao Z, Wang K, et al. Development and evaluation of (18)F-IRS for molecular imaging mutant EGF receptors in NSCLC. *Sci Rep.* 2017;7:3121.

23. Khodadust F, Ahmadpour S, Aligholikhamesh N, Abedi SM, Hosseinimehr SJ. An improved (99m)Tc-HYNIC-(Ser)<sup>3</sup>-LTVSPWY peptide with EDDA/tricine as co-ligands for targeting and imaging of HER2 overexpression tumor. *Eur J Med Chem.* 2018;144:767-773.
24. Altai M, Perols A, Karlstrom AE, et al. Preclinical evaluation of anti-HER2 affibody molecules site-specifically labeled with <sup>111</sup>In using a maleimido derivative of NODAGA. *Nucl Med Biol.* 2012;39:518-529.
25. Jiang L, Kimura RH, Miao Z, et al. Evaluation of a (<sup>64</sup>Cu)-labeled cystine-knot peptide based on agouti-related protein for PET of tumors expressing alphavbeta3 integrin. *J Nucl Med.* 2010;51:251-258.
26. Autio A, Henttinen T, Sipila HJ, Jalkanen S, Roivainen A. Mini-PEG spacing of VAP-1-targeting <sup>68</sup>Ga-DOTAVAP-P1 peptide improves PET imaging of inflammation. *EJNMMI Res.* 2011;1:10.
27. Dong C, Liu Z, Wang F. Radioligand saturation binding for quantitative analysis of ligand-receptor interactions. *Biophys Rep.* 2015;1:148-155.
28. Blumenschein GR, Jr., Mills GB, Gonzalez-Angulo AM. Targeting the hepatocyte growth factor-cMET axis in cancer therapy. *J Clin Oncol.* 2012;30:3287-3296.
29. Pool M vDG, de Vries EG. Emerging opportunities for c-MET visualization in the clinic. *J Nucl Med.* 2016;57:663-664.
30. Wu AM, Olafsen T. Antibodies for molecular imaging of cancer. *Cancer J.* 2008;14:191-197.
31. Chen K, Chen X. Design and development of molecular imaging probes. *Curr Top Med Chem.* 2010;10:1227-1236.
32. Katsila T, Siskos AP, Tamvakopoulos C. Peptide and protein drugs: the study of their metabolism and catabolism by mass spectrometry. *Mass Spectrom Rev.* 2012;31:110-133.
33. Ebenhan T, Schoeman I, Rossouw DD, et al. Evaluation of a flexible NOTA-RGD kit solution using Gallium-68 from different (<sup>68</sup>Ge)/(<sup>68</sup>Ga)-generators: pharmacokinetics and biodistribution in nonhuman primates and demonstration of solitary pulmonary nodule imaging in humans. *Mol Imaging Biol.* 2017;19:469-482.
34. Lowe VJ, DeLong DM, Hoffman JM, Coleman RE. Optimum scanning protocol for FDG-PET evaluation of pulmonary malignancy. *J Nucl Med.* 1995;36:883-887.
35. Sun Y, Ma X, Zhang Z, et al. Preclinical study on GRPR-targeted (<sup>68</sup>Ga)-probes for PET imaging of prostate cancer. *Bioconjug Chem.* 2016;27:1857-1864.

**36.** Janssen M, Oyen WJ, Massuger LF, et al. Comparison of a monomeric and dimeric radiolabeled RGD-peptide for tumor targeting. *Cancer Biother Radiopharm.* 2002;17:641-646.

**37.** Thumshirn G, Hersel U, Goodman SL, Kessler H. Multimeric cyclic RGD peptides as potential tools for tumor targeting: solid-phase peptide synthesis and chemoselective oxime ligation. *Chemistry.* 2003;9:2717-2725.

## Figures

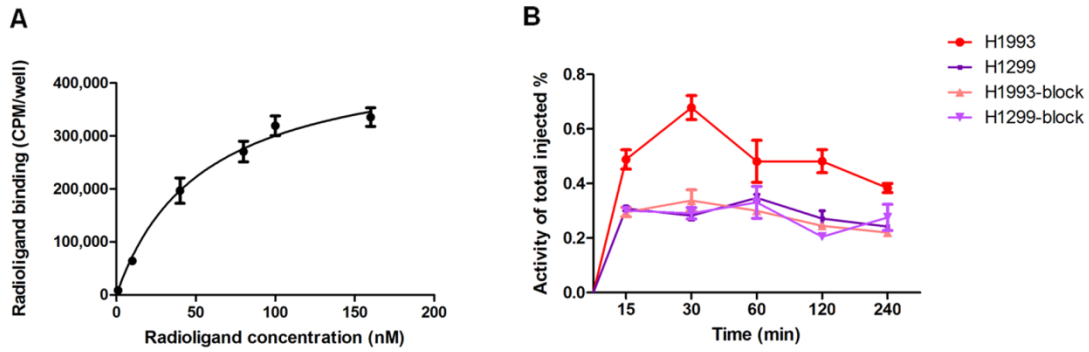


**Fig. 1** Saturation curve for binding of  $^{99m}\text{Tc}$ -HYNIC-cMBP to H1993 cells with  $K_d$  of  $56.30 \pm 2.11$  (A). Cell uptake and block-uptake of  $^{99m}\text{Tc}$ -HYNIC-cMBP in NSCLC cells (B). (CPM, counting per minute).

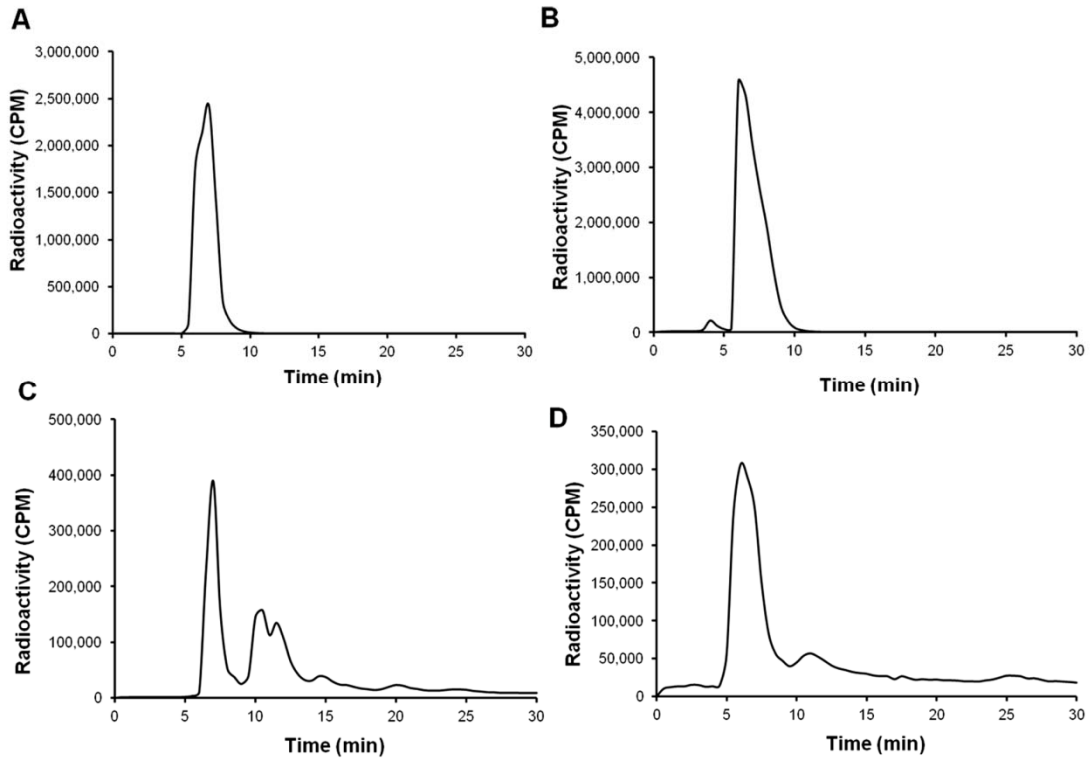


**Fig. 2** *In vivo* stability of  $^{99m}\text{Tc}$ -HYNIC-cMBP by detecting radiochemical purity in samples of plasma (A), tumor (B), liver (C) and urine (D) at 1h. (CPM, counting per minute).

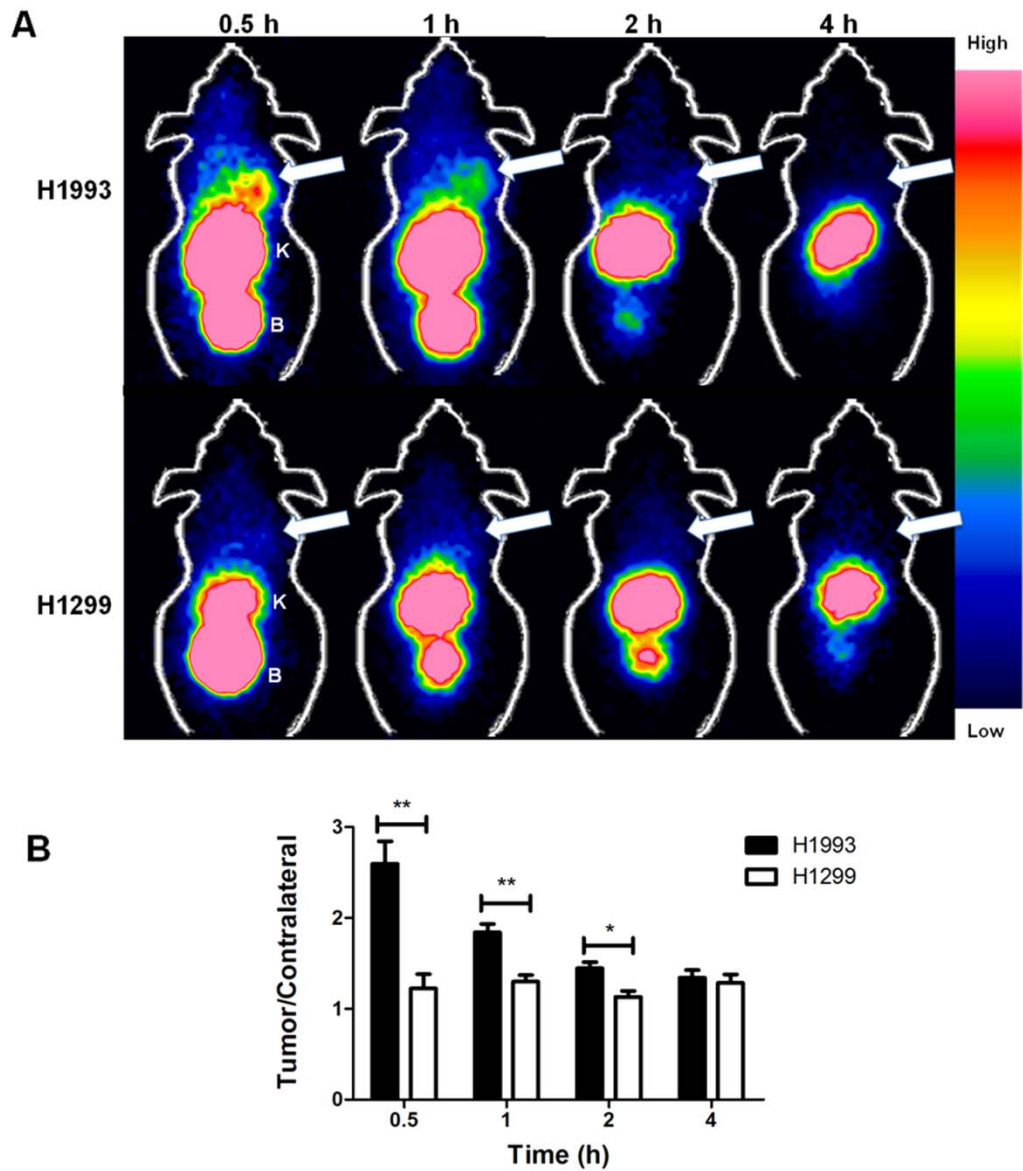


**Fig. 3** Representative coronal SPECT images of H1993 and H1299 xenografts 0-4 h after injection of  $^{99m}\text{Tc}$ -HYNIC-cMBP. White arrow indicates tumor, K indicates kidney, B indicates bladder (A). Quantitative analysis of the images was performed through counts in region of interest, \* $p < 0.05$ , \*\* $p < 0.01$  (B).

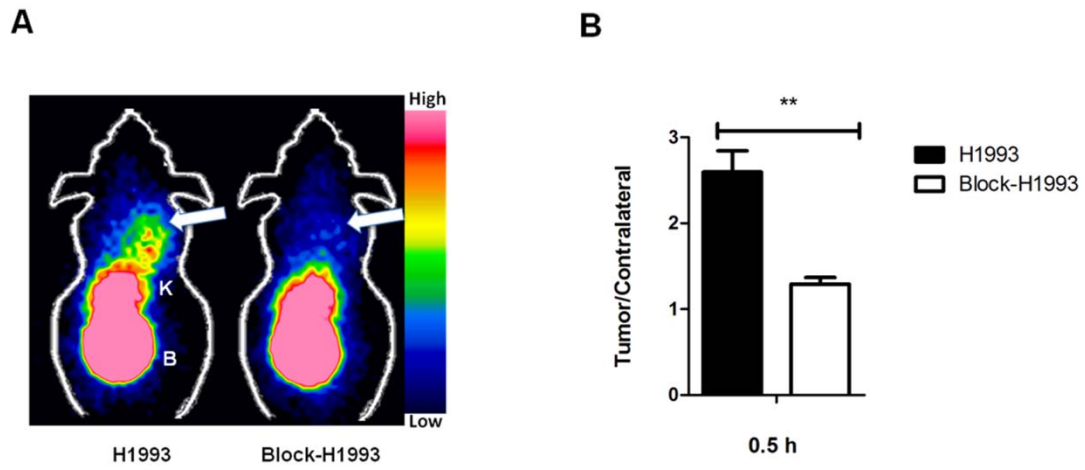


**Fig. 4** Representative coronal SPECT images for H1993 and Block-H1993 xenografts at 0.5 h. White arrow indicates tumor, K indicates kidney, B indicates bladder (A). Quantitative analysis of images was performed through counts in region of interest, \*\* $p < 0.01$  (B).

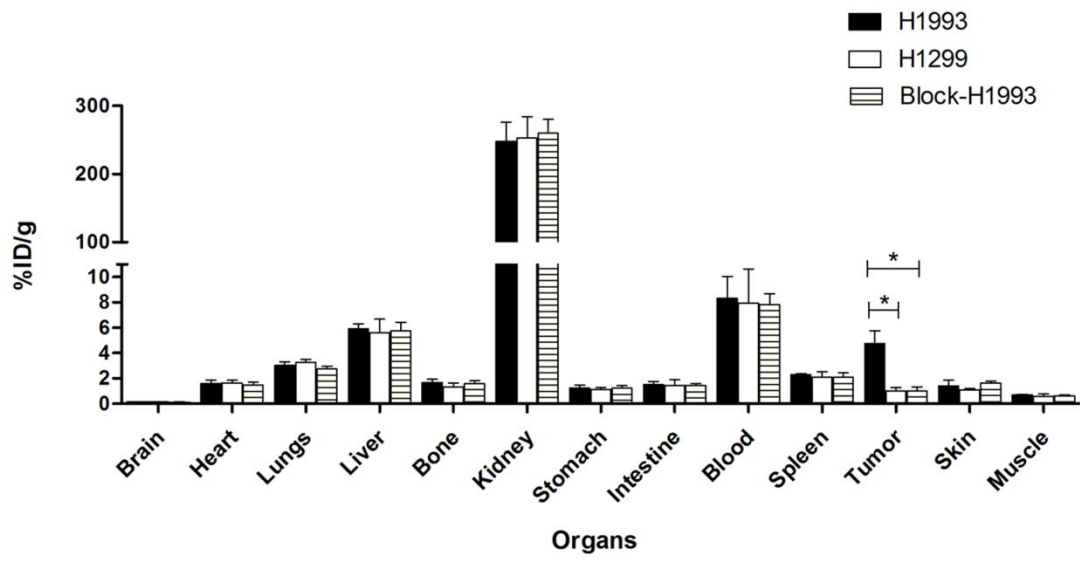


**Fig. 5** Biodistribution of  $^{99m}\text{Tc}$ -HYNIC-cMBP in H1993, H1299 and block-H1993 groups at 0.5 h after injection, \* $p < 0.05$ .

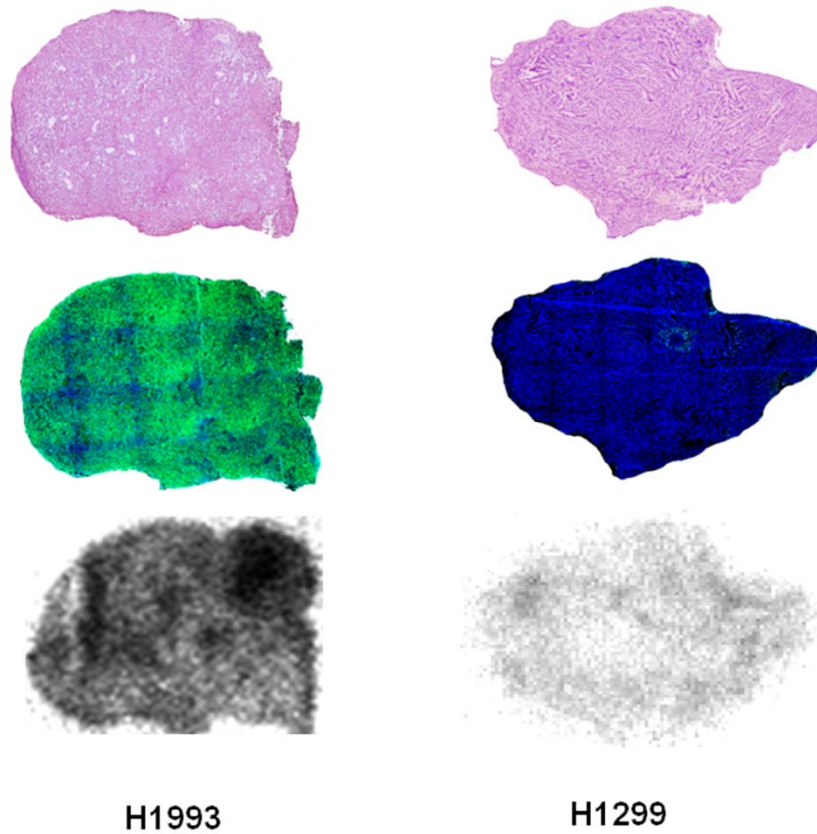
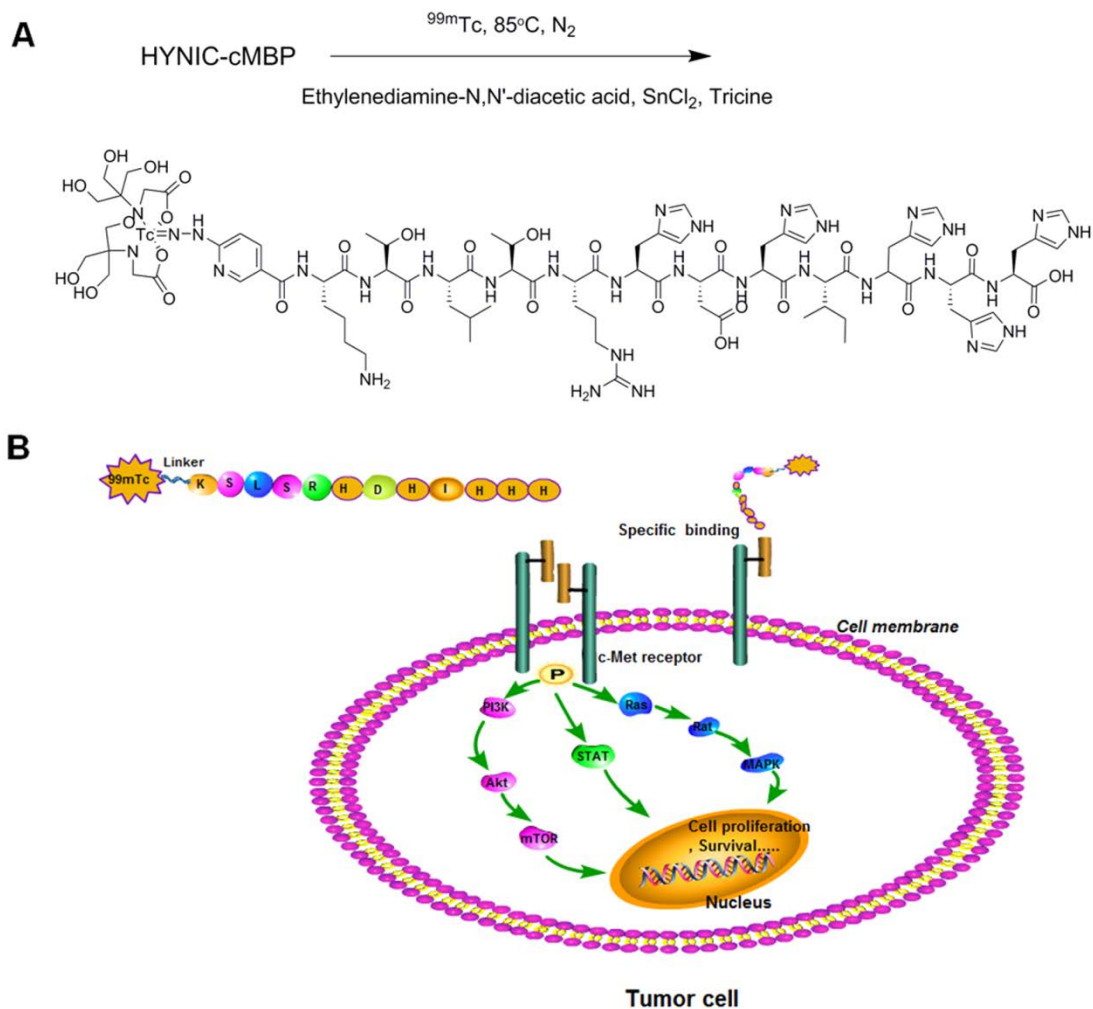
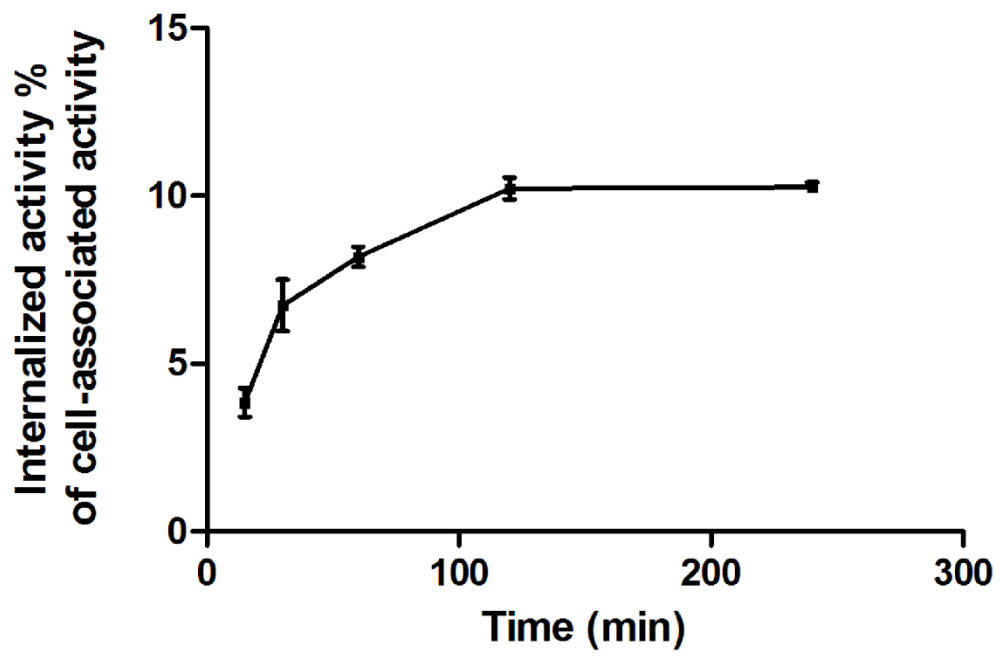


**Fig. 6** Comparison of HE staining (top row), immunofluorescence (middle row) and autoradiography images (bottom row) of H1993 and H1299 tumor sections at 0.5 h after injection of  $^{99m}\text{Tc}$ -HYNIC-cMBP. ( In immunofluorescence images, green fluorescence indicates high expression of c-Met).

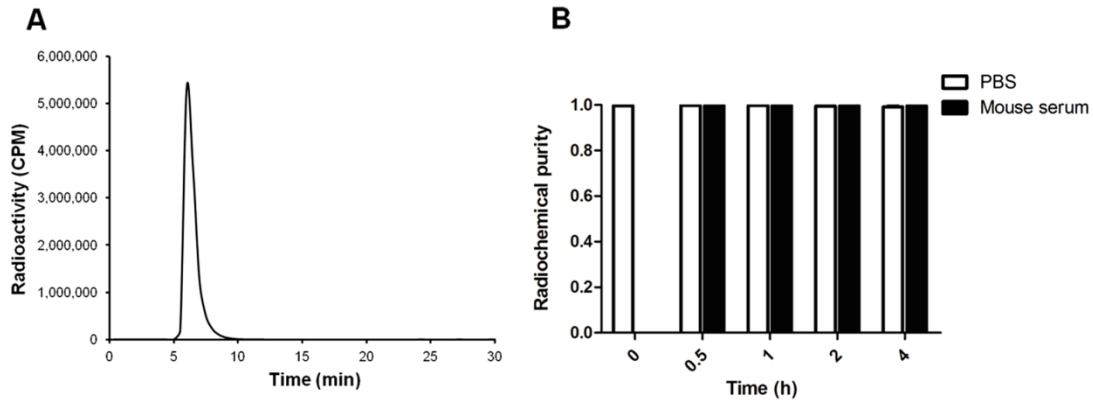
## Supplemental Data.



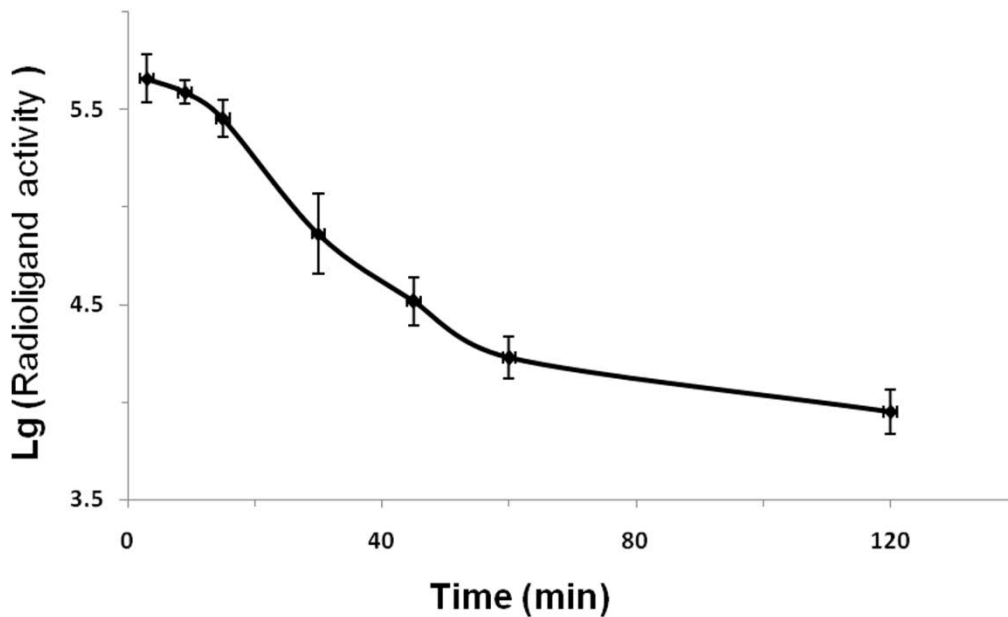
**Supplemental Fig. 1** The schematic diagram illustrates the process of radiochemical synthesis and molecular structure of  $^{99m}\text{Tc}$ -HYNIC-cMBP (A) and the specific binding of the tracer to c-Met receptor (B).



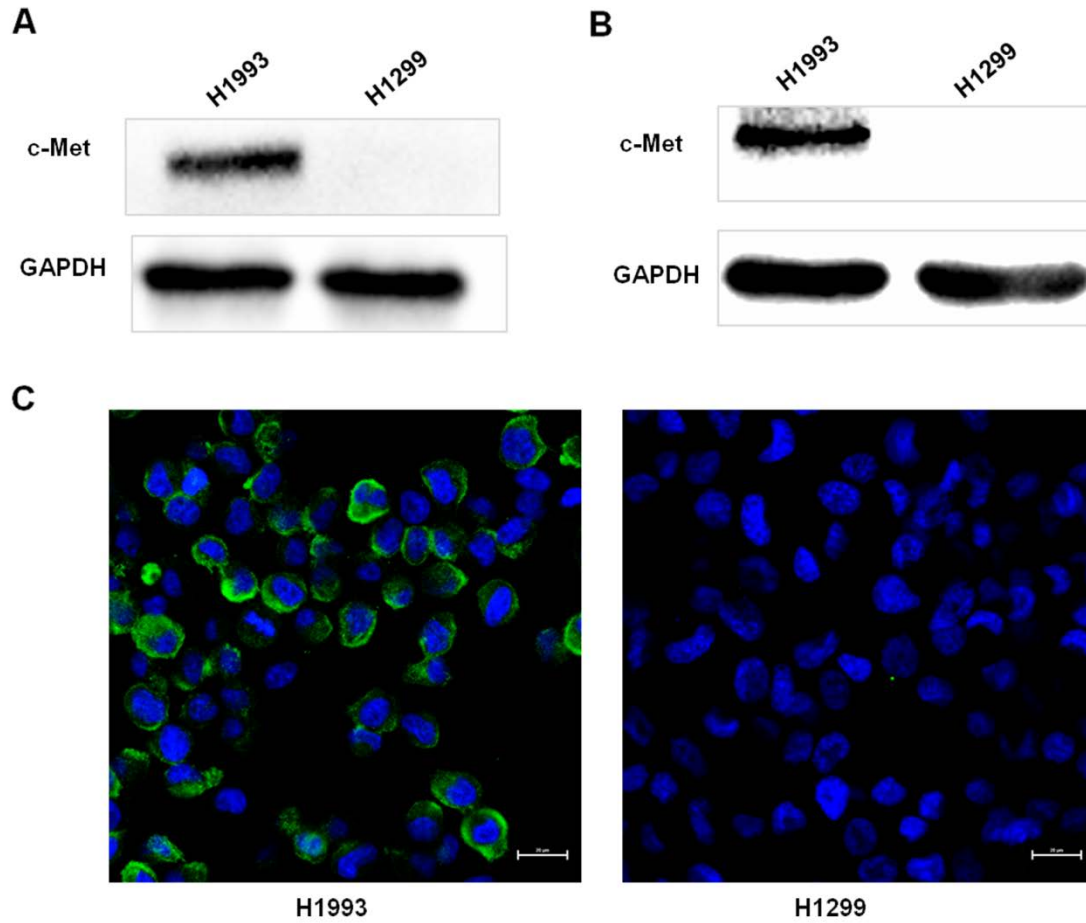
**Supplemental Fig. 2** Percent of internalized activity to cell-associated activity (membrane-bound + internalization).



**Supplemental Fig. 3** Radiochemical purity of  $^{99m}\text{Tc}$ -HYNIC-cMBP in PBS at 0 h after the tracer was prepared (A). *In vitro* stability analysis of the intact tracer by detected radiochemical purity of  $^{99m}\text{Tc}$ -HYNIC-cMBP in PBS and (or) mouse serum at 0-4 h after the tracer was prepared (B).



**Supplemental Fig. 4** Representative time-logarithmic value of activity curve of supernatant/plasma at 3, 9, 15, 30, 45, 60 and 120 min after injection of  $^{99m}\text{Tc}$ -HYNIC-cMBP.



**Supplemental Fig. 5** Western blot analysis of c-Met expression in H1993 and H1299 cell lines (A) and tumor tissues (B). Confocal images of immunofluorescence staining for c-Met expression in H1993 and H1299 cell lines (C).

**Supplemental Table 1:** Biodistribution of  $^{99m}\text{Tc}$ -HYNIC-cMBP in mice bearing H1993 tumors and in blocked H1993 groups at different time points.

Organ	0.5h		1h	2h	4h
	H1993	H1993-block			
<b>brain</b>	0.16±0.02	0.13±0.03	0.11±0.06	0.03±0.01	0.02±0.00
<b>heart</b>	1.59±0.39	1.46±0.33	0.69±0.11	0.20±0.04	0.24±0.04
<b>lung</b>	3.02±0.41	2.75±0.30	1.81±0.72	0.51±0.13	0.20±0.04
<b>liver</b>	5.92±0.57	5.75±0.95	4.92±1.36	3.75±1.57	2.58±1.52
<b>bone</b>	1.67±0.36	1.61±0.30	0.90±0.18	0.29±0.06	0.26±0.06
<b>kidney</b>	247.55±40.52	259.77±29.25	225.93±12.61	159.21±33.68	138.16±25.13
<b>stomach</b>	1.25±0.32	1.23±0.28	0.66±0.10	0.28±0.04	0.21±0.07
<b>intestine</b>	1.51±0.35	1.43±0.22	0.79±0.18	0.22±0.07	0.18±0.06
<b>blood</b>	8.32±2.45	7.80±1.25	1.99±0.19	0.72±0.37	0.83±0.08
<b>spleen</b>	2.30±0.11	2.08±0.52	1.76±0.30	1.16±0.77	1.03±0.18
<b>tumor</b>	4.74±1.43	1.03±0.43	2.84±0.28	0.87±0.13	0.75±0.14
<b>skin</b>	1.40±0.64	1.62±0.25	0.58±0.05	0.37±0.12	0.60±0.14
<b>muscle</b>	0.70±0.07	0.64±0.08	0.29±0.04	0.06±0.02	0.06±0.00

Values are mean ± SD and expressed as %ID/g (n=3)

**Supplemental Table 2:** Biodistribution of  $^{99m}\text{Tc}$ -HYNIC-cMBP in mice bearing H1299 tumors at different time points.

<b>Organ</b>	<b>0.5h</b>	<b>1h</b>	<b>2h</b>	<b>4h</b>
<b>brain</b>	0.14±0.03	0.07±0.003	0.03±0.01	0.04±0.01
<b>heart</b>	1.64±0.33	0.21±0.11	0.23±0.19	0.28±0.15
<b>lung</b>	3.26±0.33	1.65±0.39	0.46±0.29	0.32±0.10
<b>liver</b>	5.62±1.50	5.09±0.83	3.53±0.85	2.02±0.91
<b>bone</b>	1.30±0.49	0.57±0.03	0.36±0.06	0.25±0.03
<b>kidney</b>	252.66±44.37	207.49±15.19	174.14±41.35	143.95±50.02
<b>stomach</b>	1.13±0.22	0.43±0.07	0.33±0.05	0.28±0.14
<b>intestine</b>	1.45±0.65	0.69±0.31	0.21±0.05	0.21±0.03
<b>blood</b>	7.92±3.84	1.61±0.40	0.87±0.38	0.88±0.28
<b>spleen</b>	2.09±0.60	1.72±0.26	1.13±0.23	0.96±0.39
<b>tumor</b>	1.00±0.37	0.71±0.13	0.47±0.17	0.46±0.30
<b>skin</b>	1.08±0.16	0.99±0.24	0.52±0.15	0.52±0.15
<b>muscle</b>	0.57±0.27	0.22±0.03	0.08±0.03	0.06±0.03

Values are mean ± SD and expressed as %ID/g (n=3)